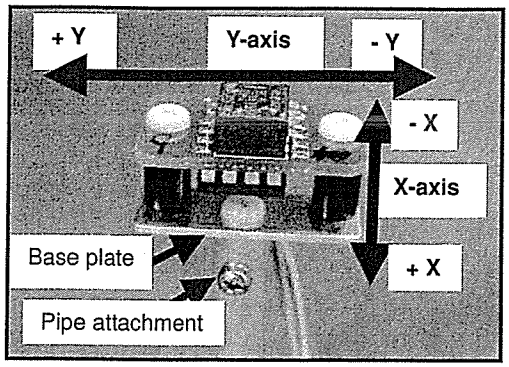

Photo 2. General outline of tilt sensor

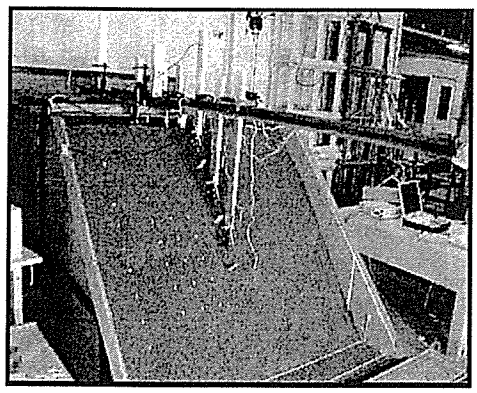

Photo 3. Setting up of instruments (Slope-I-2)

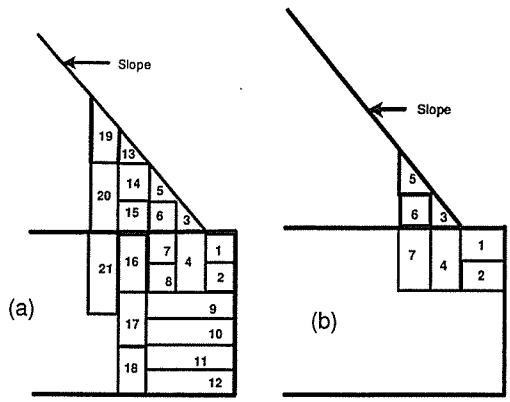

Figure 2. Steps of excavation (a) for Slope-V-1and (b) for Slope-V-2.

Target positions for the laser sensors were set up perpendicularly on the slope surface and slope top. Laser sensor and VDTs were then set up on the required positions. Movement of the slope surface measured by laser sensors is represented by S_1, S_2, S_3, etc. Similarly vertical and horizontal movement of laser sensors set up the slope top are represented by V_1, V_2, and H_1, H_2 respectively. Vertical deformation of VDTs is represented by VDT_1, VDT_2, etc. Tilt sensors were set up both on the slope surface and slope top. They were directly inserted with the tubular pipes attached at the base of the sensor. Tilt sensor placed on the slope surface is represented by A_1, A_2, A_3, etc. and those on the slope top are represented by A_4, A_5, A_6, etc. General outline of instrument set up is shown in Figs. 1(a), (b) and (c) and Photo 3. Tilt-sensors were set up near and on the same line of the laser targets.

Excavation was done manually at the bottom of the slope as shown in Fig. 2. Both toe and trench excavations were done in steps. Depth and width of each trench as well as the toe excavation were different. Between each step of excavation, about 5 minute time interval was allowed so that the movement of slopes as well as the top surface of the slope could be observed. Excavations were continued until the slope was failed. In all the tests, at first, the trench excavation was done. In case of Slope-V-1, total numbers of excavation steps were 21 where complete failure took place. In contrary, total number of steps for Slope-V-2 was 7 by which complete failure took place. Steps and elapsed timing for failure for each test are also shown in Table 1.

2.2 Centrifuge Tests and Instrumental Set Up

NIIS-centrifuge Mark-II (Horii et. al 2006) was used for the test. For the excavation of the centrifuge model slope, in-flight excavator (Toyosawa et. al 1998) was used by changing its auger with excavating blade which is 20 cm in width. Here also, River sand was used. To prepare the model slope, at first soil specimen was statically compacted with in a model box (0.45m x 0.20m x 0.272m), using bellofragm cylinder. Compaction was done under 200 kPa with 15 layers; 3 minutes of compaction time was allowed for each layer. In between each layer, Kaoline power was spread so that failure pattern could be seen clearly during failure of slope.

Once the compaction was completed, model slope ground was trimmed to its required dimension. To reduce the friction between the model sand ground and the wall of the model box, rubber membrane was used and thin film of grease was applied in between rubber membrane and apparatus wall. On the rubber membrane, 1cm X 1cm square boxes were drawn in advance so that excavation width and height could be decided while the test was under centrifuge.

Once the model box was ready, it was shifted to centrifuge platform and four direct contact type linear variable differential transducers (LVDTs) were set up on the slope surface. In-flight excavator was then lowered and set up so that its blade lies well within the model apparatus box and could move freely during the operation. Operation of in-flight excavation was done from the control room. Excavation steps for centrifuge are shown in Fig. 3, where the number represents the steps. Other than 50A, all the test models have same trench depth. As in small scale full size test, here also slopes with three angles 50, 60 and 70

degrees were prepared. Total height of each model slope ground was around 0.25m. Since the thickness of the model base is 0.04m, the height of slope becomes 0.21m. To simulate two types of slope heights as in small scale full size tests, centrifuge tests were conducted in 6g and 10g. During the centrifuge test, centrifuge acceleration was increased in two steps; 0~3~6g or 0~5~10g. Bulk unit weight, slope height, centrifuge acceleration, failure step and failure time for each test are shown in Table 2. General layout of 50, 60 and 70 degree slope models are shown in Fig. 4(a), (b) and (c) respectively. Water content of the tests was varied from 7.3 to 8.11%.

Table 2. Centrifuge model tests conditions

Test	Unit Weight	Slope Height	Centrifuge Acceleration	Failure Step	Time
	kN/m^3	m	ng		min.
50A	14.87	1.24	6	11	11.50
50B	14.96	2.06	10	9	10.49
60A	14.96	1.22	6	10	12.25
60B	14.98	2.06	10	3	3.52
70A	14.98	1.15	6	3	1.39

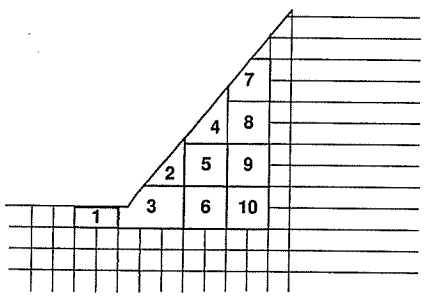

Figure 3. Excavation steps for centrifuge tests

2.3 Limit Equilibrium Analysis and Direct Shear Test

To define the cohesion and angle of shearing values to carry out the limit equilibrium analysis of centrifuge test models, direct shear test was conducted where specimens were prepared by static compaction under 200 kPa. Each specimen was prepared with four-layer compaction; each layer was compacted for 3 minutes. During the test, consolidation was done in four steps; 50, 100, 150 and 200 kPa and consolidation was stopped using 3t-method. Shearing was done at 0.02 mm/min under constant pressure.

Limit equilibrium analysis for each centrifuge test model was conducted using commercially available "Geo-Slope" slope stability analysis software. Dimension of each analysis model is same as that with in the centrifuge test for all the tests except 50A just before the failure. But in the analysis, all the centrifuge dimensions were multiplied by centrifuge acceleration during failure. Automatic determination of failure plane was selected and determined automatically. Factory of safety from the moment equilibrium using Ordinary method, Bishop's method and Morgenstern-Price (M-P) method was compared finally.

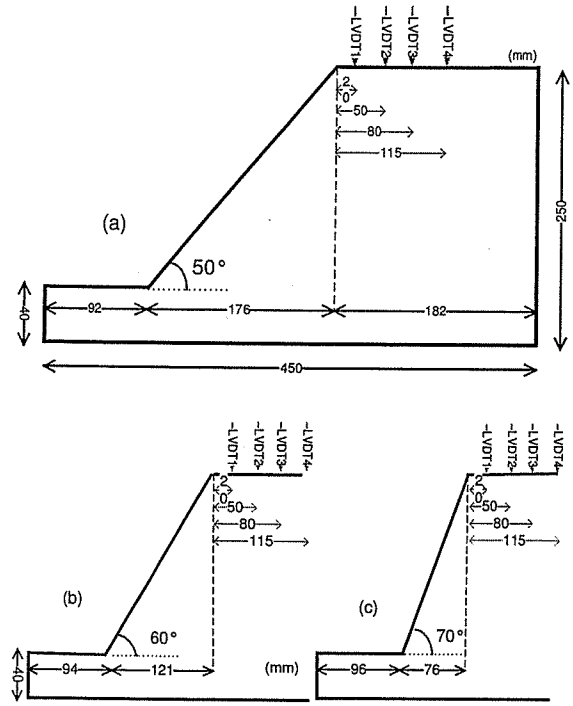

Figure 4. General layout of centrifuge slope models

3. RESULTS AND DISCUSSION

3.1 Small Scale Full Size Test

In the Figs. 5, deformations measured on the slope top of different small scale full size tests are shown. Here, V and VDT represent the vertical deformation measured by laser sensor and vertical displacement transducers. Digits followed by previous letters represent the distance from the slope crest in centimeter. For Slope-II-3 and Slope-IV-2 and Slope-V-2, deformations measured by VDTs are only shown. Comparing the total time taken for short and large slope heights for same slope angle, it could be observed that the total elapsed time for failure is longer for smaller slope heights than that for longer slope heights. Also, comparing the total elapsed time for failure for both slope heights with slope angles varying from 50 to 70 degrees, it was observed that smaller the slope angle, longer the time for failure. In all the test cases, with the increase in the excavation, gradual increment in the deformation was seen. At the beginning, it was difficult of see the clear increments, but just with the increase in excavation portion and elapsed time, large increment was observed. In all the test cases, laser and VDTs nearer to the slope crest showed the maximum and sharp movement just before the

failure. This shows the possible position for the measurement of slope movement during the excavation in order to predict the failure in advance. Movements of slope surface and slope top during the excavation and just before the failure measured by laser sensors for Slope-I-2, Slope-IV-1 and Slope-V-1 are shown in Figs. 6, 7 and 8, respectively. Bold vertical lines in the figures show the trigger for just before and after the excavation. In all the cases, it could be seen that the movement of S_1 was the maximum as it is in the closest distance from the excavation. Others gradually increase. Sharp increment just before the failure is more prominent in both the places (slope surface and slope top). Measurement of tilt angle either on the slope surface or on the slope top or both for Slope-I-2, Slope-IV-1 and Slope-V-1 are shown in Figs. 9(a), (b), 10 and 11(a), (b), (c). Although movements of each sensor for both X and Y directions were measured, here mainly movements along X direction are shown. At the beginning where small excavations were only made, clear increment in tilt angles was not seen. But after certain elapsed time, gradual increment in tilt angle was seen, which sharply increases just before the failure. Comparing the laser sensors data (including VDTs data) of Figs. 5(a), (c), (e) and Figs. 6, 7, 8 and tilt sensors data of Figs. 9, 10, 11, similar trend of movements were observed. This shows the applicability of possible measurement of slope failure pattern so that prediction of failure could be done in advance. In Fig. 11(c), movement of tilt sensors on the slope top along Y direction for Slope-V-1 is shown. Sharp increment before failure was seen. Therefore, knowing the movement along X and Y directions with tilt sensors, possible direction of failure could also be predicted in advance.

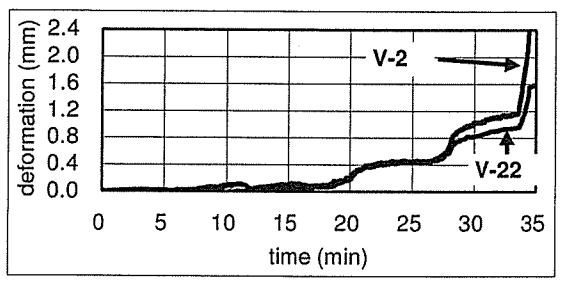

Figure 5(a). Deformation of slope top for Slope-I-2

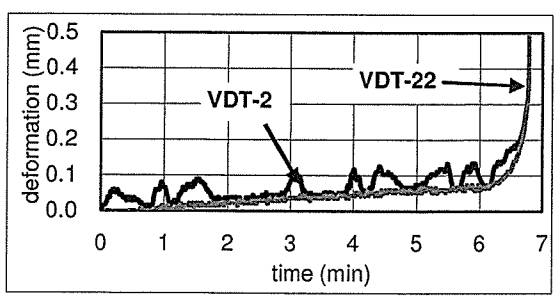

Figure 5(b). Deformation of slope top for Slope-II-3

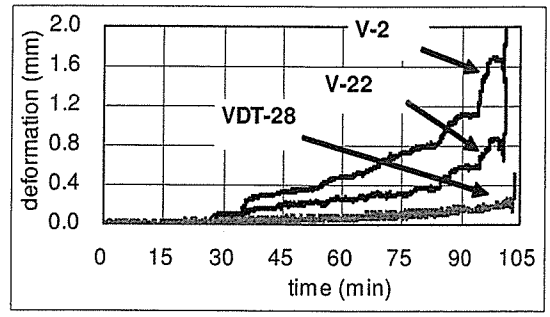

Figure 5(c). Deformation of slope top for Slope-IV-1

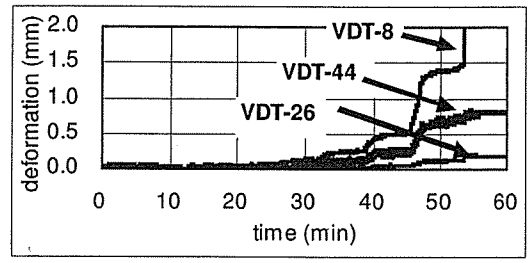

Figure 5(d). Deformation of slope top for Slope-IV-2

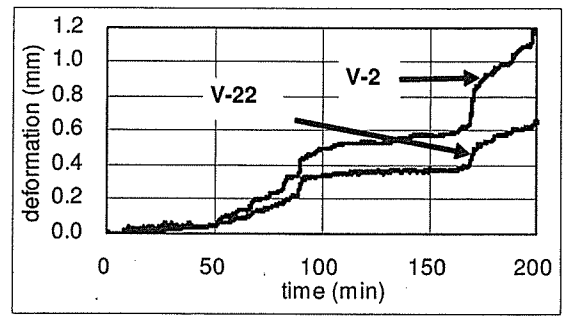

Figure 5(e). Deformation of slope top for Slope-V-1

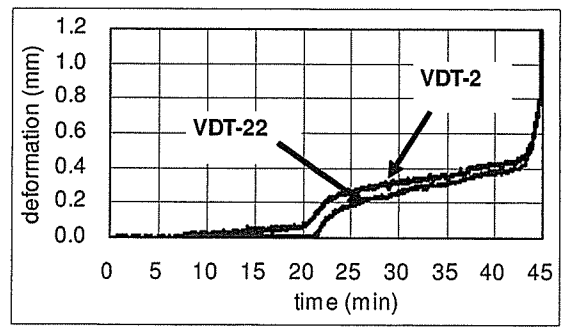

Figure 5(f). Deformation of slope top for Slope-V-2

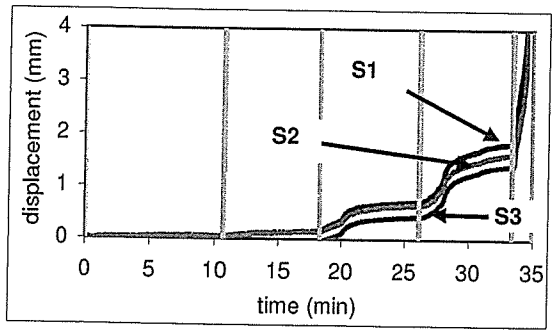

Figure 6. Movement of slope surface (Slope-I-2)

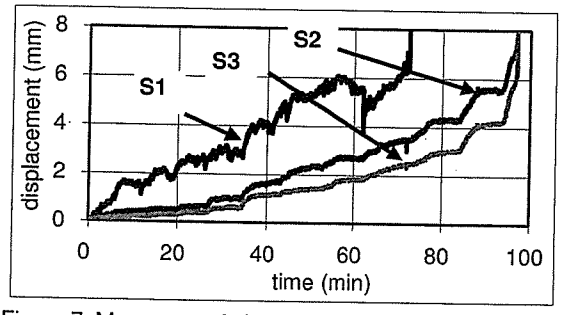

Figure 7. Movement of slope surface (Slope-IV-1)

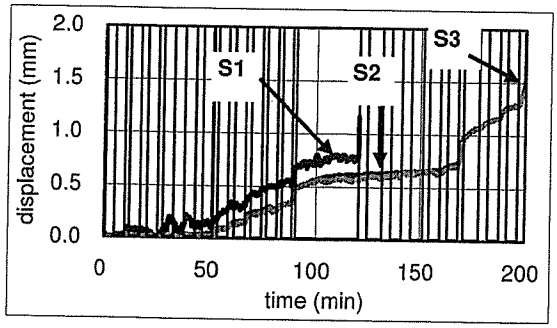

Figure 8. Movement of slope surface (Slope-V-1)

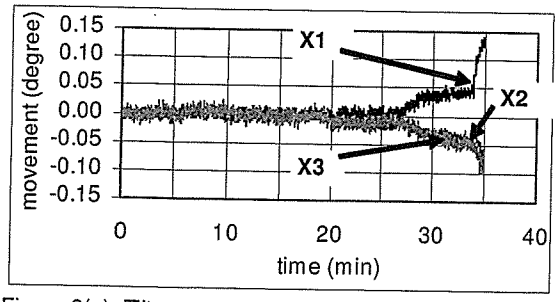

Figure 9(a). Tilt sensors on slope surface (Slope-I-2)

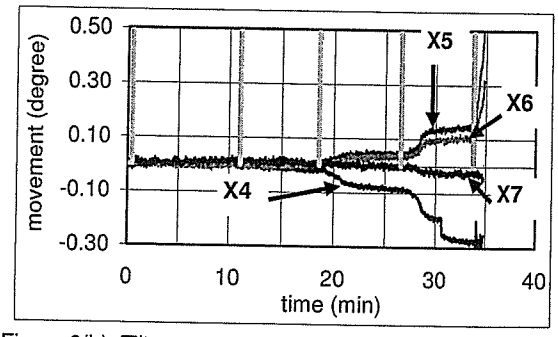

Figure 9(b). Tilt sensors on slope top (Slope-I-2)

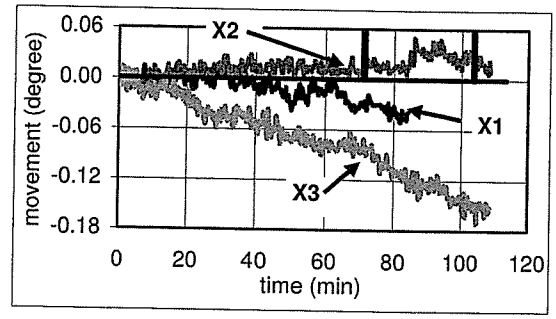

Figure 10. Tilt sensors on slope surface (Slope-IV-1)

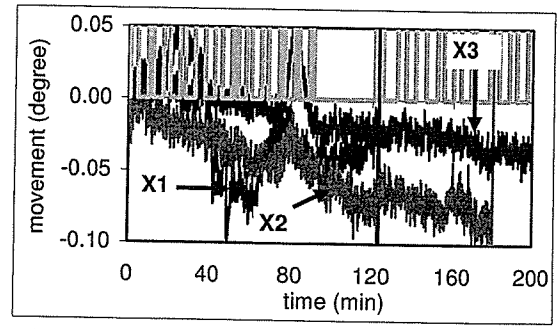

Figure 11(a). Tilt sensors on slope surface (Slope-V-1)

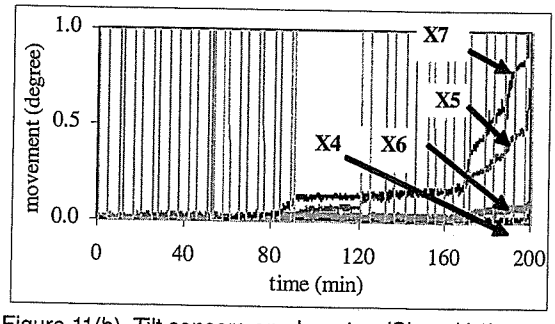

Figure 11(b). Tilt sensors on slope top (Slope-V-1)

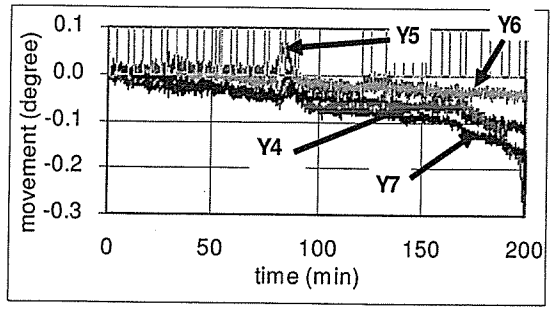

Figure 11(c). Tilt sensors on slope top (Slope-V-1)

3.2 Centrifuge Test Results

In Figs. 12, relationship between elapsed time and vertical displacement of slope top measured by LVDTs are shown. Failure step and elapsed time of failure are shown in Table 2. In all the test cases, vertical deformation increases with the increase in excavation steps. Except for case 60A (Fig. 12(c)), gradual increment in the vertical deformation; specially LVDT-1 and LVDT-2 just before the failure was seen for all the cases. Large and sharp increment in vertical deformation was seen for the cases of 50B and 60B which have larger slope height. Small or sudden failure was seen for slopes having smaller slope height (50A, 60A and 70A cases). Also, elapsed time to failure for slopes having higher slope height is longer than slopes having smaller slope height.

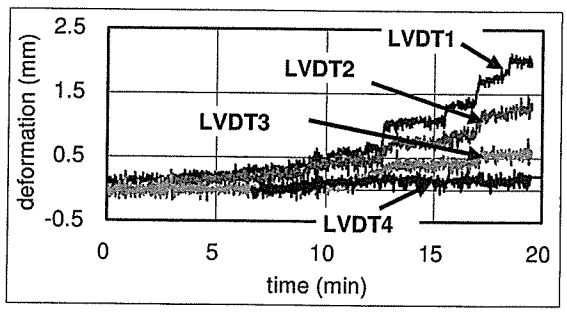

Figure 12(a). Deformation on slope top (50A)

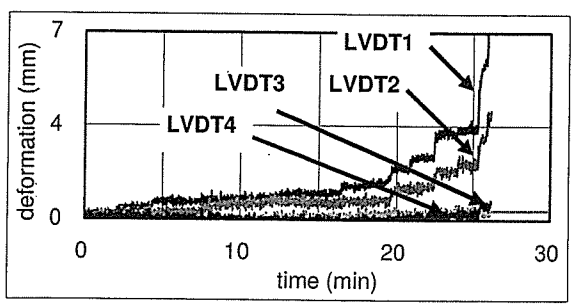

Figure 12(b). Deformation on slope top (50B)

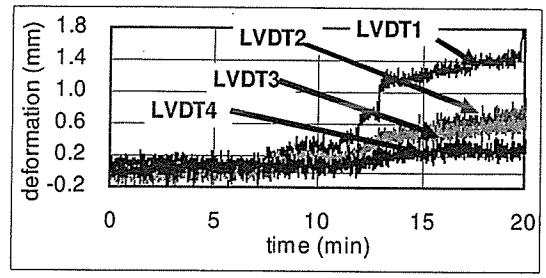

Figure 12(c). Deformation on slope top (60A)

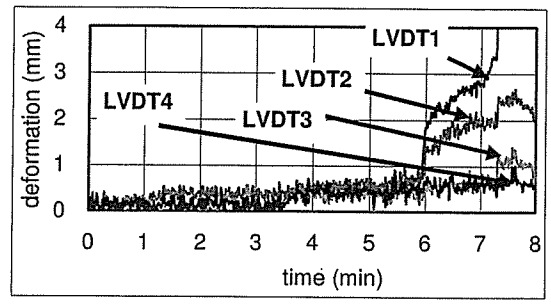

Figure 12(d). Deformation on slope top (60B)

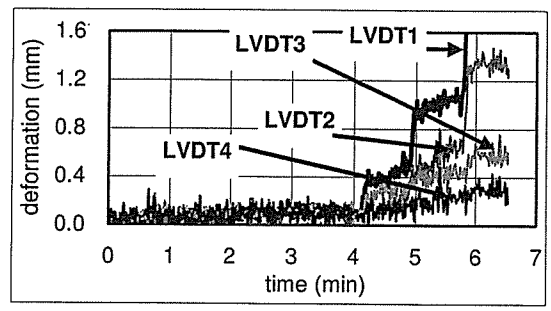

Figure 12(e). Deformation on slope top (70A)

Comparing the slope angles (50, 60 and 70 degrees), it was seen that the slopes having higher slope angle failed sooner than those having smaller slope angles. Number of excavation (steps) carried out up to failure also decreases with the increase in the angle of slope. Also, amount of deformation before the failure was larger for 50A than 60A and 70A, 70A showing the minimum value. Therefore, it could be said that slopes having higher slope angle and larger slope height fails sooner than those having smaller slope angle and smaller slope height. Similar results were seen in small scale full size tests also. This is due to weight of the slope behind the cut which increases with the increase in slope angle and slope height. More sharp increment in LVDTs was seen for 50B and 60B in comparison to 50A and 60A just before the failure. This means that for higher slopes, movement of slope is very faster and quicker than those for smaller height slopes. As

explained earlier, soil mass behind the excavation (cut) might have affected the movement of the slope.

3.3 Limit Equilibrium Analysis Results

Effective angle of cohesion and effective angle of frictional resistance measured from the direct shear test were 2.09 kPa and 37.22 degrees, respectively. These values were used in limit equilibrium analysis. Figure 13 shows the failure plane obtained from limit equilibrium analysis for 60A. Factor of safety (F.S.) obtained for all the tests are shown in Table 3. Slopes 50B, 60A, 60B and 70A were failed with F.S. value around 1.03 to 1.13. During the centrifuge test also, failure was occurred with the same amount of excavation. Factor of safety in case of 50A slope was around 1.26 to 1.28, showing the lesser possibility of complete failure. Partial failure was seen for 50A case during the centrifuge test also. Factor of safely around 1 obtained from limit equilibrium analysis showed that the centrifuge test results have good resemblance with the analysis data.

Figure 13. Failure plane from analysis (for 60A)

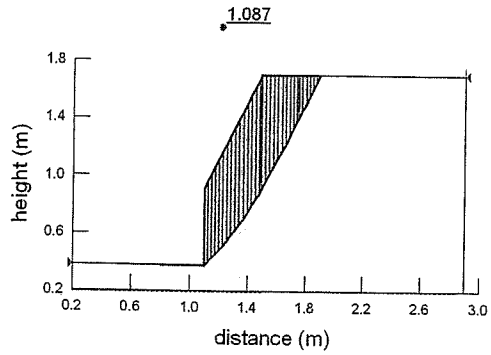

Table 3. Factor of safety from limit equilibrium analysis.

Method	50A	50B	60A	60B	70A
Ordinary	1.28	1.13	1.09	1.04	1.13
Bishop	1.26	1.13	1.08	1.03	1.12
M-P	1.27	1.13	1.09	1.03	1.13

5. CONCLUSIONS

From the small size full scale tests, following conclusions could be withdrawn;

1. With the step and time of excavation, movement of slope surface and deformations of the slope top could be measured from the start to the end of the excavation using laser sensors and vertical displacement transducers. Measurement of steep and sharp changes in the movement and deformation just before the failure showed the possibility of measurement of failure in advance.

2. Tilt-sensor also gave the gradual response with the time and step of excavation. Sharp and steep changes in the tilt angle both on the slope surface and slope top just before the failure was possible to measure. The trend of movement of tilt sensors is similar to the movement and deformation of laser sensor and vertical displacement transducers. This showed the possible application of tilt sensors in the excavation field for the prediction of failure in advance. With X and Y direction movements, possible direction of failure could also be predicted.

3. LVDTs used to measure the deformation of slope top in the centrifuge tests showed the graudual increment with elapsed time of excavation. Comparing the deformation amount of LVDTs on the centrifuge top, it was seen that the maximum movement was observed for the LVDTs set up at the nearest to the crest. This shows the possible position for the measurement of deformation

4. In both the small scale full size tests and centrifuge teste, slope having larger slope angle showed the quicker failure and smaller deformation in comparison to slopes which have small slope angle. Similarly, slopes with larger slope height showed shorter elapse time for failure than those with smaller slope height. Also, deformation pattern just before the failure for slopes having higher slope height are more steep and sharp than those for smaller height slopes.

5. Factor of safety obtained was around 1.03 to 1.13 except for 50A which is around 1.28. Since the analysis was carried for centrifuge model test just before the failure, it varifies that centrifuge test resutls are appropriate.

ACKNOWLEDGEMENT

This research is partially carried out under the Health and Labor Sciences Research Grants of Ministry of Health, Labor and Welfare. Authors are also thankful to Mr. Taiki Kasama of Hokkaido University for his help during centrifuge tests. Thanks are also extended for Akebono Brake Industries Co. Ltd., Tokyo for her support in preparing the tilt sensors.

References

Horii N., Itoh K, Toyosawa Y., and Tamate S. (2006) Development of the NIIS Mark-II Geotechnical Centrifuge, *International Conference on Physical Modelling in Geotechnics*, Hongkong (under print).

Toyosawa, Y., Horii, N., & Tamate, S. (1998) Deformation and failure behavior of anchored retaining wall induced by excessive excavation in centrifuge model tests, *Research Reports of the National Institute of Industrial Safety*, (NIIS-RR-97):35-46.

INVESTIGATION OF SLOPE FAILURE DURING TRENCH EXCAVATION IN PEAT GROUND

Timpong Sahaphol, National Institute of Industrial Safety, Tokyo, Japan
Toyosawa Yasuo, National Institute of Industrial Safety, Tokyo, Japan
Tamrakar Surendra Bahadur, National Institute of Industrial Safety, Tokyo, Japan
Itoh Kazuya, National Institute of Industrial Safety, Tokyo, Japan
Horii Noriyuki, National Institute of Industrial Safety, Tokyo, Japan

ABSTRACT
This paper presents the investigation of slope failure that occurred during trench excavation in peat ground. Site investigations in collaboration with in-situ and laboratory tests were conducted in order to investigate the cause of slope failure. The deterministic and probabilistic slope stability analyses were carried out to evaluate the slope stability and the probability of failure. In addition, a series of centrifuge modelling was conducted to verify the mechanism of slope failure. Based on site investigations, slope stability analyses and centrifuge tests conducted in this paper, the cause of slope failure was attributed to the excessive surcharge load of excavated materials that stockpiled on the top of the slope.

RÉSUMÉ
Cette thèse présente la recherche sur une rupture de talus qui s'est produite pendant une excavation de tranchée sur sol tourbeux. Des investigations sur le site ont été conduits conjointement avec les essais in-situ et en laboratoire afin de trouver la cause de la rupture du talus. Des analyses de stabilité du talus déterministes et probabilistes ont été effectuées pour évaluer la stabilité du talus et la probabilité de rupture. En outre, une série de modélisations centrifuges a été conduite pour vérifier le mécanisme de rupture du talus. S'appuyant sur les investigations sur le site, les analyses de stabilité de talus et les essais centrifuges effectués dans cette thèse, la cause de la rupture du talus a été attribuée à la surcharge de matériaux excavés stockés au sommet du talus.

1. INTRODUCTION

In Japan, it was reported that during the period of 1989 to 2001 approximately 15 to 30 workers were killed every year due to the slope failure incidents (Toyosawa et al. 2005). In this paper, three workers were killed in the trench due to the slope failure. The construction site was located in the northern area of Japan. This construction project consists of temporary trench excavations for burying the water pipelines in the agriculture areas. The trench was excavated up to approximately 4 m to 4.5 m depth and formed a 0.6H:1V trench wall slope. According to the geologic survey map, the construction site was located in the natural ground consisting mainly of peat. In general, trench excavation in peat ground often encounters difficulties in design and construction due to a high compressibility and a low strength of peat. A preliminary investigation was carried out including taking photographs and interviewing the eyewitness to obtain more understanding of the conditions prior to, during and subsequent to the slope failure. This paper presents the findings from the site investigation, laboratory tests, slope stability analyses and centrifuge modelling test. The results provide insight into the possible cause and the mechanism of slope failure.

2. SITE INVESTIGATION

After the failure, land surveying was conducted around the area of slope failure. Figure 1 shows the surface topography and the location of slope failure. Due to the rescue operation between the stations S4 and S5, some parts of collapsed grounds were removed. However, at the adjacent station S3, the collapsed grounds were almost undisturbed. The water pipeline was observed in the collapsed ground, which might be uplifted during the slope failure. Therefore, it was considered that the slope failure occurred from the top through the toe of the slope. In order to examine the subsurface condition, three test borings were drilled nearby the failure location as presented in the Figure 1. In addition, the in-situ tests including the cone penetration test (CPT) and the standard penetration test (SPT) were also carried out in order to obtain the soil properties.

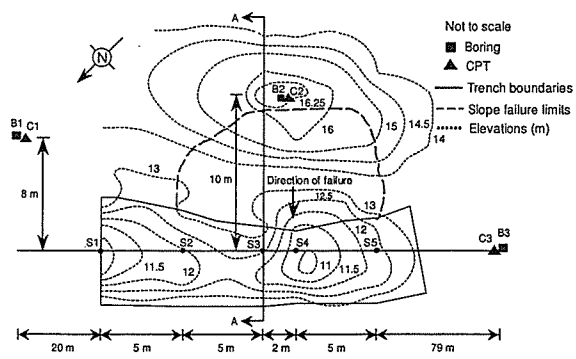

Figure 1. Plan view of the slope failure

2.1 Subsurface Condition

Figure 2 shows the cone penetration test results. Soil samples collected from the borings were tested in the laboratory to determine the physical properties such as natural water content, soil consistency and unit weight for soil classification. Undisturbed soil samples were also collected and carefully transported to the laboratory for determining the shear strength. The estimated subsurface conditions in the slope failure area are presented in Figure 3, which is a cross section AA at the station S3 and soil properties are summarized in Table 1. The upper deposit consists of about 4 to 4.5 m thick layer of peat. Relatively high natural water content can be observed in this layer, this is probably due to the fact that peat samples have a highly fibrous fabric and contain many roots which can absorb a lot of water. The peat samples have pH value of about 5, this acidity probably caused by the presence of carbon dioxide and humic acid arising from peat decay. The degree of decomposition of peat samples classified by the Von Post method ranges from moderately decomposed peat (H5) to strongly decomposed peat (H7) (H1 is totally undecomposed peat and H10 is completely decomposed peat). Underlining the peat layer is a deposit of silt layer with a thickness of about 1 to 1.5 m. The fine sand layer is encountered below the silt layer, this fine sand can be classified as a loose ground (N = 5). The observed ground water level is approximately 0.9 m below the ground surface. According to the consistency test results, the natural water contents for peat and silt layers are much higher than the plastic limit and very close to the liquid limit. Generally, soil with the natural water content near or higher than the liquid limit will behave more like a liquid than a solid, and such a soil will have a relatively low shear strength which may result in the instability of slope.

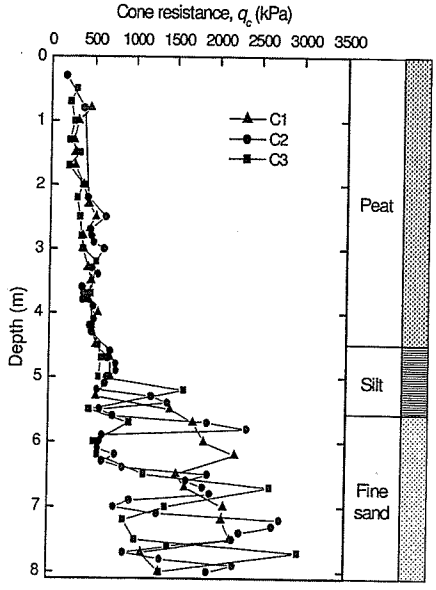

Figure 2. Cone penetration test results

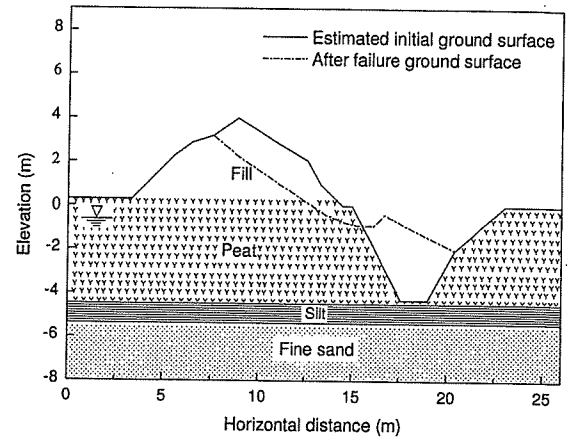

Figure 3. A schematic view of the cross section AA

Table 1. Summary of soil properties.

Depth (m)	Soil	w (%)	LL (%)	PL (%)	γ (kN/m^3)	N
0-4.5	Peat	127-483	134-341	61-143	11.5	0-3
4.5-5.6	Silt	40-116	46-81	25-40	17	3-5
5.6-8.0	Fine sand	37-40	41-44	25-28	17	5

Note: w = water content, LL = liquid limit, PL = plastic limit, γ = unit weight, N = standard penetration number

2.2 Determination of Undrained Shear Strength

The unconfined compression test (UU test) is commonly used to determine the undrained shear strength of saturated cohesive soils. The undrained shear strength, c_u can be calculated by the following equation.

$$c_u = q_u / 2 \quad [1]$$

where q_u is the unconfined compression strength. The undrained shear strength of silt was determined using the Eq. 1. However, in case of peat, sometimes it is difficult to determine the undrained shear strength by the unconfined compression test especially when the peat specimen fails under plastic failure mode, in which the specimen bulges laterally into a barrel-shape without shear plane. According to the Japan Geotechnical Society (2004), the undrained shear strength of peat can be approximately determined from the cone resistance, q_c in the cone penetration test by the following equation.

$$c_u = q_c / 20 \quad [2]$$

For the fine sand layer, the friction angle, ϕ was estimated by the penetration number, N obtained from the standard penetration test as follows (Dunham 1954)

$\phi = 15+(12\times N)^{0.5}$ [3]

The average undrained shear strength parameters for peat, silt and fine sand layers are summarized in Table 2. It should be noted that the undrained shear strength for peat was taken as the average value obtained from the unconfined compression and cone penetration tests.

Table 2. Summary of the shear strength parameters.

Soil type	c_u (kPa)	ϕ (°)
Fill	12	-
Peat 1 (0-2 m)	12	-
Peat 2 (2-4.5 m)	23.5	-
Silt	26	-
Fine sand	-	23

3. SLOPE STABILITY ANALYSIS

3.1 Back Analysis of Slope Failure

The slope stability is conventionally analyzed in terms of factor of safety, FS. The factor of safety is defined as the ratio of the available shear strength along the critical failure surface to the shear stress acting on the surface. Because the permeability of peat layer is relatively low, at the end of the excavation the soils will be virtually in the undrained condition and a total stress analysis will be relevant. According to the eyewitness interviews, the day prior to the slope failure, the excavated materials had been dumped and formed an embankment on the top of the slope. By considering the equilibrium of the collapsed ground volume, the initial condition prior to the failure can be estimated as shown in the Figure 3.

Back analysis of the undrained shear strength for peat and silt layers by Morgenstern's Price method was performed at the cross section AA, the analysis results are shown in Table 3. The undrained shear strength along the failure plane was calculated using FS = 1.0 for instant slope failure. It should be noted that the undrained shear strength of the excavated materials was assumed to be the same as the upper peat layer (0-2 m depth) and soil above ground water table was also considered as a saturated soil. The back calculated undrained shear strengths are slightly lower than those observed in the laboratory and the in-situ tests. This indicates that the assumption of a circular failure surface and estimation of ground condition prior to slope failure provide sufficient accuracy for the slope stability analysis.

Table 3. The back calculated undrained shear strengths.

Soil type	Back calculated c_u (kPa)
Fill	11
Peat 1	11
Peat 2	20
Silt	26

3.2 Probabilistic Slope Stability Analysis

One of the disadvantages with the use of the minimum factor of safety obtained from the conventional slope stability analysis is that it does not imply the probability of failure due to the uncertainty of the input parameters used in the analysis especially the input soil parameters. To overcome this limitation, the uncertainty parameters can be accounted for by considering the slope stability in terms of probability analysis. In the probabilistic slope stability analysis, the soil parameters were assumed to be characterized statistically by a normal distribution defined by minimum, maximum, mean and standard deviation obtained from the in-situ and laboratory testing results as shown in Table 4. The Monte Carlo simulation was used to compute a probability distribution of the factor of safety as implemented in the program SLOPE/W. The probability of failure, PF is determined by counting the number of safety factors below 1.0 and then taking this number as a percentage of the total number of converged Monte Carlo trials (Kranh 2004). According to the sensitivity analysis result, the unit weight of soil was found to be least significant input parameter for determining the stability of slope. Consequently, in the probabilistic slope stability analysis, the unit weight of soil was held constant.

Table 4. Statistical parameters of the undrained shear strength.

c_u (kPa)	Peat 1	Peat 2	Silt
Minimum	4	15	22
Maximum	23	32	34
Mean	12	23.5	26
Standard deviation	5	4	4

In general, a factor of safety of 1.1 is generally accepted as the minimum value for the stability of a temporary slope, which will be backfilled after the completion of work. Based on the analysis result, the probability of failure is about 23.71% and the minimum deterministic factor of safety by Morgenstern's Price method is 1.13. It is considered that the probability of failure is not acceptable since the factor of safety is slightly greater than the acceptable factor of safety (FS = 1.1). In addition, the probability of failure is also higher than the allowable probability of failure (PF = 10%) for temporary structures as proposed by Santamarina et al. (1992).

3.3 Effect of Excavated Materials

The deterministic and probabilistic slope stability analyses were performed in order to investigate the effect of excavated materials on the slope stability. Surcharge loads from the excavated materials (γ = 11.5 kN/m^3) were applied on the top of slope with different heights (H), widths (W) and side clearances (S) as illustrated in Figure 4. It should be noted that the slope 1H:1V of the embankment was held constant and the subsurface condition was the same as shown in the Figure 3. Figure 5 shows the relationship between factor of safety and

embankment height. The factor of safety gradually decreases with an increase in the embankment height and the factor of safety becomes lower than the acceptable factor of safety (FS < 1.1) when the embankment height is higher than 3 m with the side clearance of less than 0.5 m. In addition, the slope with a longer embankment width shows a lower factor of safety for a given embankment height. The relationship between probability of failure and embankment height is presented in Figure 6.

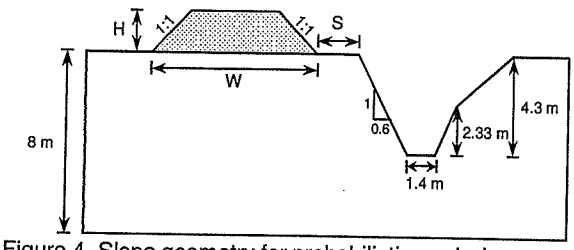

Figure 4. Slope geometry for probabilistic analysis

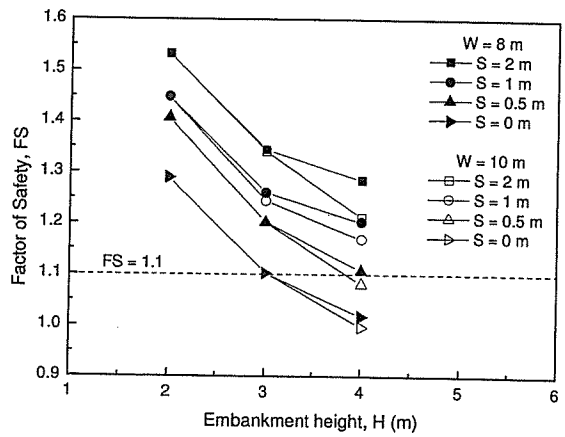

Figure 5. Relationship between FS, S and H

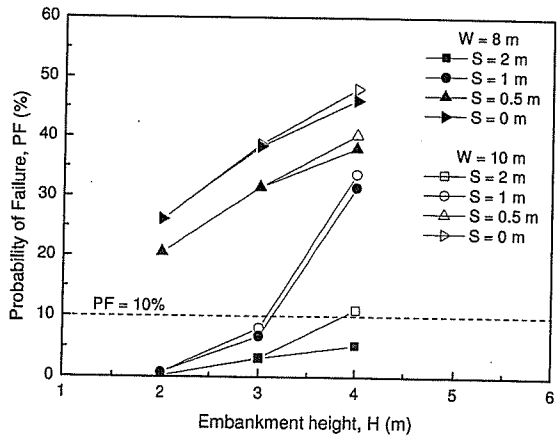

Figure 6. Relationship between PF, S and H

As can be seen in the figure, the probability of failure increases with the embankment height and the probability of failure is higher than the allowable probability of failure (PF > 10%) when the embankment height becomes higher than 3 m with the side clearance of less than 1 m.

4. CENTRIFUGE MODELLING

A wide range of geotechnical problems can be investigated by the geotechnical centrifuge modelling. In this paper, the mechanism of slope failure was evaluated using the Mark-II centrifuge at the National Institute of Industrial Safety (NIIS). The NIIS Mark-II centrifuge has an effective radius of 2.3 m with a maximum acceleration capacity of 100g. It is capable of simulating the dynamic and static geotechnical problems. The detail and specification of the NIIS Mark-II centrifuge were described by Horii et al. (2006).

4.1 Model Preparation

In order to simplify the ground model, the silt and sand layers were eliminated from the model. This is reasonable, since the critical slip surface pass through the silt layer only a short distance. The model test was performed in a rigid model box with a transparent Plexiglas sidewall to enable side viewing of the model during centrifuge flight. The internal dimensions of the rectangular model box are 150×450×272 mm. It is common to use the same soil in the model test as in the prototype. However, in case of peat ground which contains many different sizes of roots and fibers, it is extremely difficult to use the natural peat in the centrifuge test due to the effect of scaling laws. During the increasing of centrifuge acceleration, the size of fibers and roots will increase by *n* times of gravity. For example, peat with a 5 mm diameter root tested at the centrifuge acceleration of 50g, the root diameter will become 25 cm corresponding to the prototype scale. In order to overcome this problem, the peat ground model was prepared by mixing the slurry of Kaolin (NSF clay) and a very small size of sawdust as a ratio of about 4:3 by weight at 200% water content in the mixing machine for about 1 hour.

After the mixing, the slurry was placed into the model box and pre-consolidated under a consolidation pressure of about 10 kPa. By this method, relatively high water and organic content and low density can be achieved in the peat ground model which is consistent well with the natural peat ground. The resulting block of the peat ground model was trimmed to form the trench geometry. The embankment of excavated material was prepared in another container by static compaction using the bellofram cylinder. The embankment was trimmed to a desired geometry and then placed on the top of the peat ground model. To observe the deformations of the slope during the centrifuge flight, the target markers were embedded into the model at equally space intervals. The sidewall friction of the model box was reduced by lubricating the sidewalls with the silicone grease. Figure 7 shows a schematic view of the experimental model setup

and the arrangement of linear variable displacement transducers (LVDTs). The digital video camera and CCD camera were installed in front of the model box to provide a continuous record of the ground model during the centrifuge test.

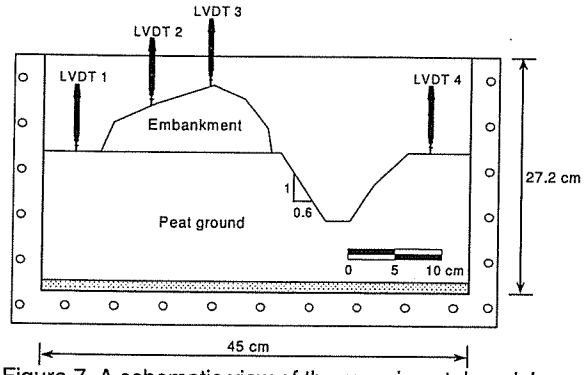

Figure 7. A schematic view of the experimental model

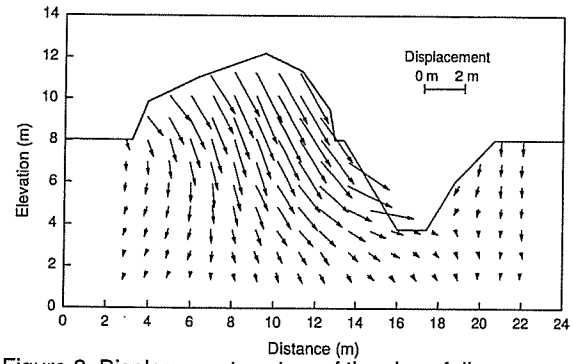

Figure 8. Displacement vectors of the slope failure

4.2 Experimental Results

After the model box was loaded onto the centrifuge swinging platform, the centrifuge acceleration level was gradually increased until the undrained slope failure was observed. Upon reaching an acceleration level of about 25g, the failure mechanism was initiated by the horizontal movement of ground towards the slope face. The complete slope failure was observed at the acceleration of about 54g, where the slope model geometry are corresponding to the prototype geometry. Two-dimensional deformations of the ground model can be evaluated by measuring the displacement of each marker captured by taking photographs through the transparent Plexiglas sidewall during the centrifuge test. The coordinate of each target was determined by a digitizer software. Figure 8 shows the displacement vectors of the model after slope failure, the maximum displacement is about 2.75 m corresponding to the prototype scale. The distribution of maximum shear strain ($\gamma_{max} = \varepsilon_1 - \varepsilon_3$) after the slope failure is also presented in Figure 9. Large maximum shear strain can be observed from the toe of the slope towards the embankment. From the centrifuge test result, it verified that the surcharge load from the excavated materials induced the large deformation which resulted in the instability of slope.

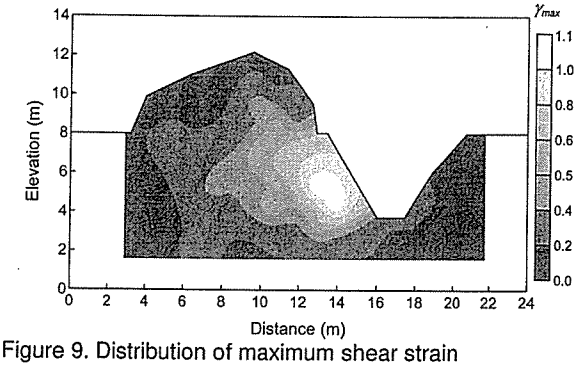

Figure 9. Distribution of maximum shear strain

5. CONCLUSIONS

In this paper, the geotechnical investigation, slope stability analyses and the centrifuge modelling were conducted in order to investigate the cause of slope failure. The back calculated shear strengths were found in good agreement with the values obtained from in-situ and laboratory tests. The instability of slope was clearly observed from the low factor of safety and the high probability of failure. In addition, the large deformation and failure of the slope due to the excessive surcharge load was also observed in the centrifuge test. This emphasized that the cause of slope failure was probably due to the excessive surcharge load of the excavated materials that stockpiled on the top of the slope. However, because the deformation-strength characteristic of peat ground during the excavation was not fully investigated, further research on this point should be conducted in order to prevent this type of accident.

References

Dunham, J.W. (1954) Pile foundation for buildings, *Proc. ASCE Soil mechanics and foundation division.*

Horii, N., Itoh, K., Toyosawa, Y. and Tamate, S. (2006) Development of the NIIS Mark-II geotechnical centrifuge, *Int. Conf. on Physical Modelling on Geotechnique, Hong Kong.* (in press)

Japan Geotechnical Society (2004) Geotechnical manual for Peat, *Geotechnical note*, 14. (in Japanese)

Kranh, J. (2004) *Stability modelling with SLOPE/W: An engineering methodology*, Alberta, Canada.

Santamarina, J., Altschaeffl, A. and Chameau, J. (1992) Reliability of slopes: Incorporating Qualitative Information, *Transportation Research*, 1343: 1-5.

Toyosawa, Y., Itoh, K., Tamrakar, S.B. and Horii, N. (2005) Characteristics of labour accidents caused by slope failure, *Int. Symp. Landslide Hazards in Orogenic Zone*, Nepal, 1: 281-290.

STABILITY OF TRENCH EXCAVATION UNDER CONSTRUCTION MACHINERY LOAD

Toyosawa Yasuo, National Institute of Industrial Safety, Tokyo, Japan
Yang Junjie, Ocean University of China, Qingdao, China
Timpong Sahaphol, National Institute of Industrial Safety, Tokyo, Japan
Itoh Kazuya, National Institute of Industrial Safety, Tokyo, Japan
Tamrakar Surendra Bahadur, National Institute of Industrial Safety, Tokyo, Japan

ABSTRACT
Trench collapse causes a considerable number of deaths and injuries of workers every year in Japan. In this paper, a series of centrifuge modelling was conducted in order to examine the stability of trench excavation under the construction machinery load. The NIIS in-flight excavator was used to simulate the trench excavation process during the centrifuge test. In addition, the effects of ground condition, magnitude and location of the construction machinery load on the failure mechanism were also investigated. The centrifuge test results clearly revealed that the mechanism of failure was mainly controlled by the magnitude of the machinery load and the bearing capacity of ground.

RÉSUMÉ
Les effondrements de tranchées engendrent un nombre considérable des morts et blessés chez les ouvriers tous les ans au Japon. En cette thèse, une série de modélisations centrifuges a été conduite afin d'examiner la stabilité de l'excavation de tranchée sous la charge des engins de construction. L'excavatrice embarquée NIIS a été utilisée pour simuler le processus d'excavation de tranchée pendant l'essai centrifuge. En outre, les effets de l'état au sol, de l'importance et de l'emplacement de la charge des engins de construction sur le mécanisme de rupture ont également été étudiés. Les résultats des essai centrifuges ont clairement montré que le mécanisme de rupture était principalement contrôlé par l'importance de la charge des engins et la portance du sol.

1. INTRODUCTION

There are many labor accidents in which the workers are killed and buried under collapsed ground when the construction machinery such as a drag shovel falls or topples over the edge of the trench during excavation. Photograph 1 shows the example of the ground collapse during the trench excavation. Based on the labor accident reports, during the period of 1994 to 2002, there were approximately 30 workers killed every year in Japan due to this type of failure. To prevent the loss of life and injury caused by the ground collapse, it is necessary to gain more understanding about the effect of construction machinery load, geometry of ground excavation (e.g. slope angle and excavation depth) and characteristic of ground strength on the stability of trench excavation. Geotechnical centrifuge modelling is commonly accepted as a powerful tool for studying a wide range of geotechnical problems. The stability and failure mechanism of ground excavations have been investigated using the centrifuge modelling by many researchers (Kusakabe 1982, Taylor 1984 and Toyosawa et al. 1994). However, the stability and failure mechanism of trench excavation under the construction machinery load have not been fully investigated. Therefore, in this paper, a series of centrifuge modelling tests was conducted on various types of ground models under different magnitudes and locations of the machinery load in order to examine the stability and the failure mechanism of trench excavation under the construction machinery load.

Photograph 1. Ground collapse during trench excavation

2. CENTRIFUGE MODELLING

In this paper, a series of centrifuge tests was performed using the Mark-II centrifuge in the centrifuge test laboratory of the National Institute of Industrial Safety (NIIS). The NIIS Mark-II centrifuge has an effective radius of about 2.3 m with a maximum acceleration of 100g and 50g under the static and dynamic conditions, respectively. The detail of the NIIS Mark-II centrifuge was described by Hori et al. (2006). The centrifuge tests were conducted on ground models at the centrifuge acceleration of 30g and test results were presented in the model scale.

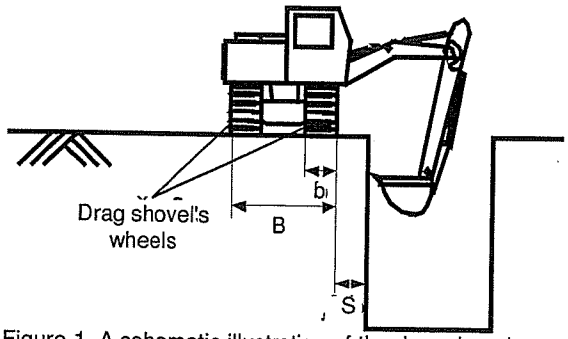

Figure 1. A schematic illustration of the drag shovel

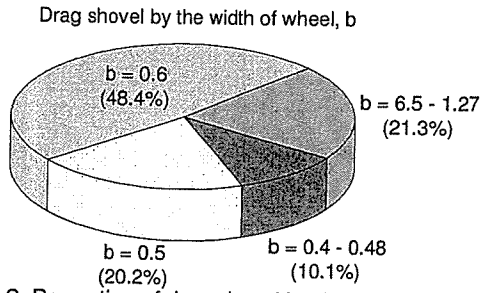

Figure 2. Proportion of drag shovel by the width of wheel

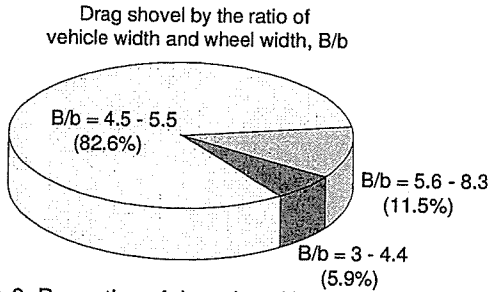

Figure 3. Proportion of drag shovel by the B/b ratio

2.1 Modelling of Construction Machinery Load

Figure 1 shows a schematic illustration of the drag shovel which is commonly used in trench excavation, the geometry of the drag shovel such as a full width of vehicle or crawler (B), a width of wheel (b) and a side clearance from the slope crest (S) are also presented in the figure. Based on the investigation of 287 different types of the drag shovels used in the trench excavation, the specifications of the drag shovel including the vehicle width, the width of wheel and the bearing pressure of the wheel can be characterized as shown in Figures 2 and 3. The bearing pressure of wheel or crawler is in the range of 9.8 to118 kPa. Figure 2 shows the proportion of the drag shovel by the width of wheel, b. It was found that the width of wheel distributes in the range of 0.4 to 1.27 m and approximately 50% of the drag shovels have the width of wheel of 0.6 m. Figure 3 shows the proportion of the drag shovel by a ratio of the vehicle width and the width of wheel, B/b. As can be seen in the figure, about 83 % of the drag shovels have the vehicle width of about 5 times of the width of wheel. Therefore, in this paper, the construction machinery load was modelled by a rigid block (U-shape) with b = 0.6 m (in prototype scale) and B/b = 5 as shown in Figure 4. It should be noted that the machinery load was modelled under the static condition.

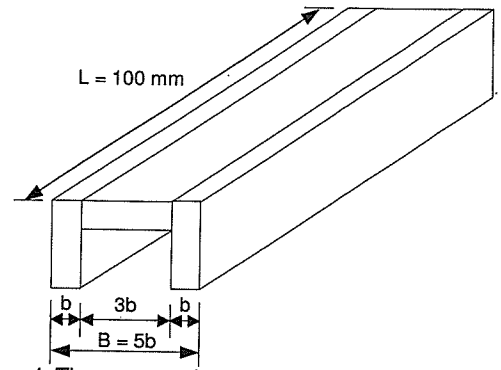

Figure 4. The construction machinery load model

2.2 Ground Model Preparation

The ground model was prepared in a rigid model box (internal dimensions of 100 mm in width, 450 mm in length and 272 mm in height) with a transparent Plexiglas front wall in order to provide side viewing of the ground model during the centrifuge test. The membrane was attached onto the ground model and silicone grease was smeared between the sidewall of model box and the membrane to reduce the sidewall friction. Three different kinds of ground models were prepared, namely, uniform sand ground model (model A), layered sand ground model (model B) and Kanto loam (a volcanic cohesive soil in Japan) ground model, (model C). The preparations of the ground models are described as follow.

Ground model A: the uniform sand ground model was prepared by pluviating air-dried Toyoura sand from a sand hopper through air at a controlled drop height into the rigid model box. Toyoura sand is classified as a uniform clean fine sand with a mean grain size, D_{50} = 0.18 mm and a density of soil particle, ρ_s = 2.65 g/cm^3. By this method, homogeneous dense sand ground model with a relative density, D_r of about 78% was obtained. The ground model was saturated by soaking the ground model in the water for about 24 hours. After the saturation process, the water content, w of the ground model of 21.6 % was obtained. In order to examine the degree of saturation, S and the water content of the ground model at the centrifuge test condition (at acceleration of 30g), the ground model was placed onto the centrifuge swinging platform and the centrifuge acceleration was gradually increased to the acceleration of 30g. It was found that the degree of saturation and the water content decreased with time and the water content and the degree of saturation remained unchanged after 15

minutes (w = 3.2%, S = 15.2%). The density of the ground model was about 1.620 g/cm^3. After the centrifuge test, the water content was measured at every 5 cm depth from the ground surface and uniform value of the water content was observed.

Ground model B: the layered sand ground model was prepared by the same material and method as used in the ground model A. However, after pluviating Toyoura sand into the model box to a thickness of approximately 10 mm, the pouring hole of the sand hopper was closed. The ground surface was levelled and the colored-dyed Toyoura sand was then placed on the ground surface with a thickness of about 5 mm in order to highlight the deformation and the location of failure surface. Thereafter, the pouring hole was reopened and the next ground layer was prepared using the same method described above. The water content and the degree of saturation of the ground model were consistent well with that of the ground model A, and the density of the layered sand ground model after the test was about 1.605 g/cm^3.

Ground model C: the Kanto loam with the particle size passing the 2 mm sieve was used in this ground model. The water was sprayed and mixed with the Kanto loam to provide the conditions of optimum water content in advance. The ground model was placed into the model box and compacted under a pressure of 49 kPa by the bellofram cylinder. For the first ground layer with a thickness of about 70 mm, the Kanto loam of 2500 g was compacted for 30 minutes. For the next ground layers, the Kanto loam was compacted in layer of about 7.5 mm thick for a total of 18 layers. After each compaction, a thin layer of air-dried kaolin powder was placed on the ground surface for the observation of the failure surface. By this method, the relative density, the wet density, and the water content of the ground model were about 66 %, 119% and 0.928 g/cm^3, respectively. After completion of the preparation of ground models, the construction machinery load model was then placed on the top of the ground surface at the specific location. The typical experimental model is shown in Figure 5.

2.3 Characteristics of Ground Models

In order to evaluate the strength of the ground models, the small-sized cone penetration test and the bearing capacity tests were conducted in the centrifuge test. The small-sized cone penetrometer has a diameter of 5 mm with a base area and a tip angle of 0.196 cm^2 and 60 degrees, respectively. Figure 6 shows the cone penetration test results for the ground model A, B and C, the cone resistance increased linearly with depth and centrifuge acceleration level for the uniform sand (model A) and the layered sand (model B) ground models. It should be noted that the test result was presented corresponding to the model scale. As expected, the ground model B has a lower cone resistance than that of the ground model A for a given centrifuge acceleration. This is mainly due to the weakness of the colored sand layers. In contrast, in case of Kanto loam ground model (model C), the uniform ground strength can be observed in which slope of the cone resistance-depth curve drop at the depth of about 20 mm and the cone resistance remains unchanged with depth. In addition, the cone resistance of the ground model under the 1g gravity field and the centrifuge acceleration of 30g are almost identical.

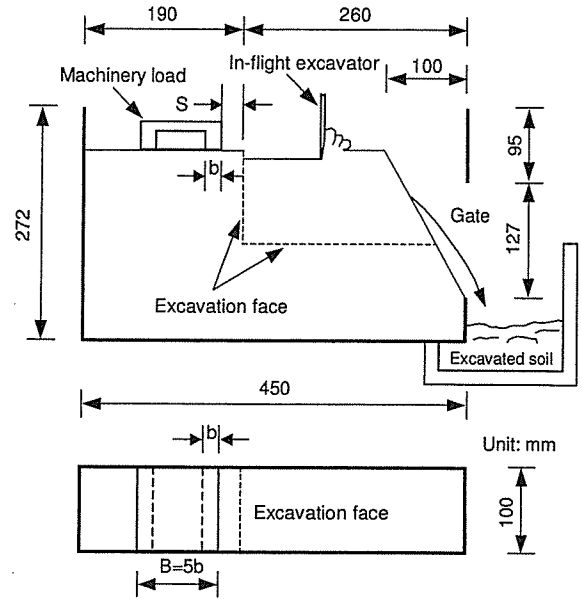

Figure 5. Typical experimental model setup

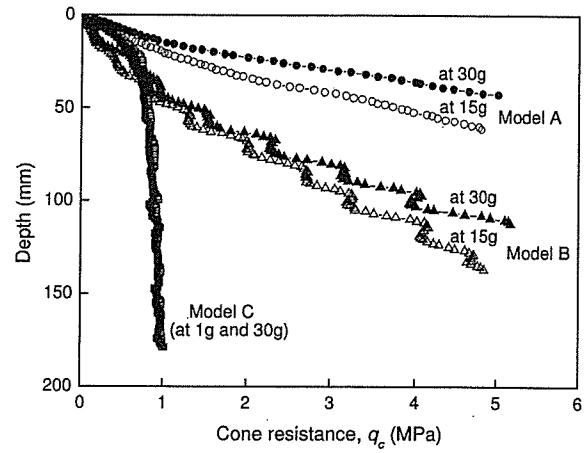

Figure 6. The cone penetration test results

This behavior may be attributed to the fact that the overburden pressure due to the self-weight of ground at the acceleration of 30g is lower than that of the preconsolidation pressure of 49 kPa, therefore, the effect of the acceleration level seems to be insignificant. The bearing capacity tests with a footing model of 20 mm in width (Bm) were conducted at the centrifuge acceleration

of 30g. The test results for the ground model A, B and C are presented in Figure 7, the bearing capacity, q is plotted with the normalized settlement, S_m / B_m. As can be seen in the figure, the ultimate bearing capacity of 1230 kPa and 700 kPa are observed in the ground model A and B, respectively. It is obvious that the ground model C has the lowest ultimate bearing capacity (91 kPa) when compare with the other ground models.

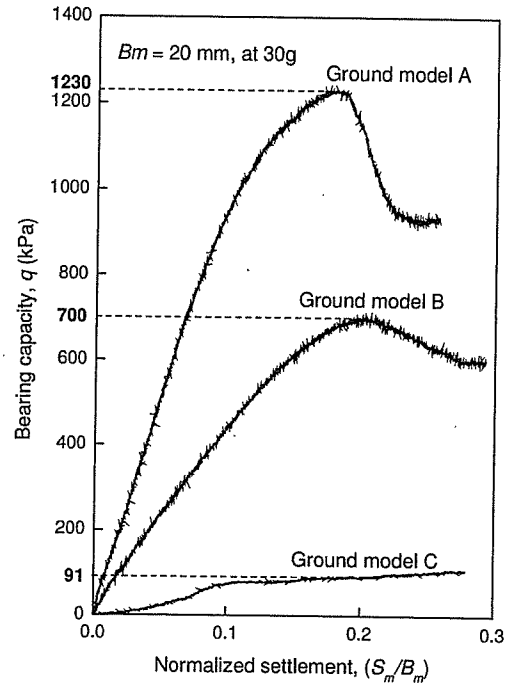

Figure 7. The bearing capacity test results

2.4 Test Conditions

A series of centrifuge tests was conducted on the three different ground models under different magnitudes and locations of the construction machinery load. The test conditions are summarized in Table 1. In addition, the centrifuge tests were also conducted on the ground models without the machinery load for the comparison.

Table 1. Summary of the test conditions

Ground model	b (mm)	Bearing pressure (kPa)	S/b
A	20	35.4	0.5,0.75,1.25,1.75
B	20	35.4	0.5,0.75,1.25,1.75
C1	20	35.4	1.25
C2	20	91.7	0.5,0.75,1.25,1.75

As can be seen in the Figure 7 and the Table 1, the bearing pressure of the machinery load (35.4 kPa) is small very about 3% and 5% of the ultimate bearing capacity of the ground model A and B, respectively. While in the ground model C1, the bearing pressure of the machinery load is about 40% of the ultimate bearing capacity. In order to see more clearly the influence of the bearing pressure on the stability of trench excavation, the machinery load model with the bearing pressure of about the same as the ultimate bearing capacity of ground was used in the model C2.

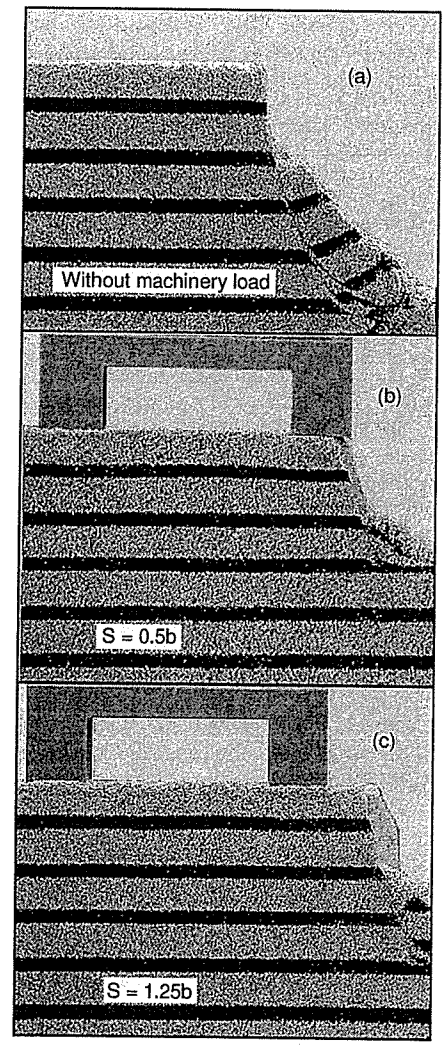

Photograph 2. Ground model B after failure, (a) without machinery load, (b) with machinery load S = 0.5b and (c) with machinery load S = 1.25b

2.5 Test Procedures

After completion of the experimental model setup, the ground model was loaded onto the centrifuge swinging platform and the centrifuge acceleration was then increased gradually until the acceleration of 30g. The NIIS in-flight excavator (Toyosawa et al. 1998), which is

capable of excavating the ground model during the high centrifuge acceleration environment was used in this paper for simulating the trench excavation process. After the centrifuge acceleration reached 30g, the ground model was excavated vertically with a thickness of about 5 mm until the ground failure can be observed. The excavation depth at just before the ground failure was recorded and defined as the maximum excavation depth.

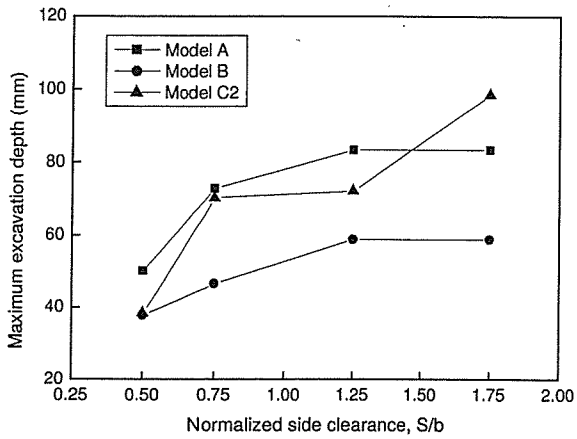

Figure 8. Relationship between the maximum excavation depth and the side clearance, S/b

3. EXPERIMENTAL RESULTS

3.1 Failure Mechanism of Sand Ground

Photograph 2(a) shows the cross-section of the ground model B after the failure in case of no machinery load, and photographs 2(b) and (c) are the example of the failure pattern of the ground model B under the machinery load. The failure pattern of ground model A is identical with that of the ground model B even the photographs are omitted here. It is obvious from the photographs that the failure mechanism is mainly due to the instability of slope. This may be attributed to the fact that in case of the sand ground models (models A and B) the bearing pressure of the machinery load is relatively small when compare to the ultimate bearing capacity of ground. Therefore, the self-weight of ground plays the important role on the instability of slope.

Figure 8 shows the relationship between the maximum excavation depth and the normalized side clearance, S/b of the ground model A, B and C2. The maximum excavation depths of the ground model A and B in case of no machinery load are 83 mm and 58 mm, respectively. It is apparent that the maximum excavation depth increases with the side clearance in the ground model A and B. However, when the side clearance is more than 1.25b, the influence of the side clearance on the maximum excavation depth seems to be insignificant in which the maximum excavation depth under the machinery load is almost the same as in case of no machinery load.

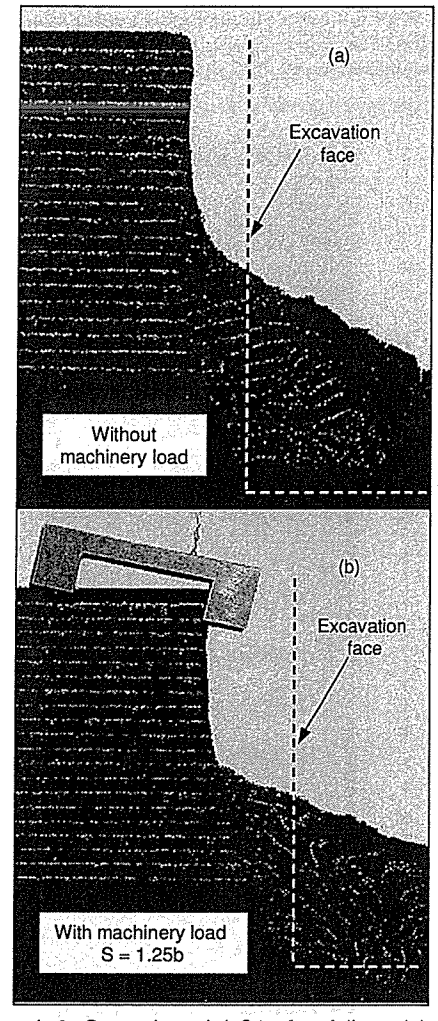

Photograph 3. Ground model C1 after failure, (a) without machinery load and (b) with machinery load S = 1.25b

3.2 Failure Mechanism of Kanto Loam Ground

Photograph 3(a) shows the failure pattern of the ground model C1 in case of no machinery load. The maximum excavation depth of about 220 mm was observed after the failure. Photograph 3(b) shows the failure pattern of the ground model C1 under the machinery load. The bearing pressure of the machinery load is about 40% of the ultimate bearing capacity of ground. The machinery load model was hung with the iron wire in order to prevent the damage of the failure pattern due to the falling of machinery load model after the failure. The maximum excavation depth of about 180 mm was observed at S = 1.25b. By comparing the photographs 3(a) and (b) the failure patterns of the ground model C1 with and without the machinery load are almost identical. In addition, the mechanism of failure is similar to that of the sand ground models in which the instability of slope is a major cause of failure. On the other hand, in case of ground excavation under the machinery load with the bearing

pressure equal to the ultimate bearing capacity of ground (model C2), the failure mechanism is totally different as can be observed in Photographs 4(a), (b) and (c).

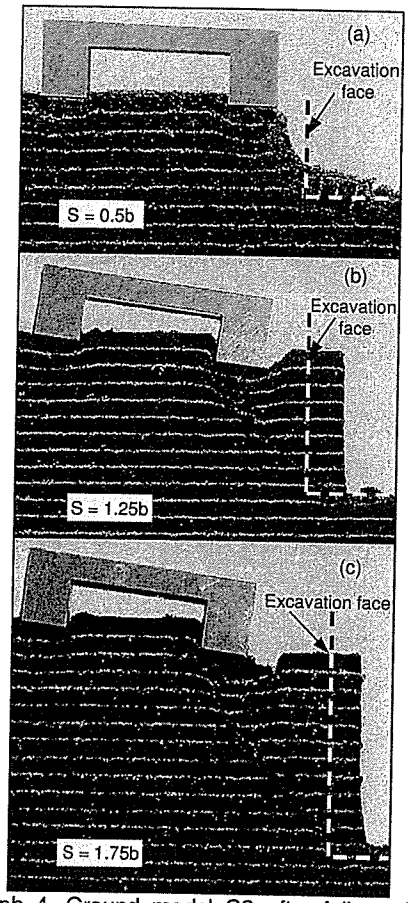

Photograph 4. Ground model C2 after failure, (a) S = 0.5b, (b) S = 1.25b and (c) S = 1.75b

Figure 9 shows the schematic illustrations of the failure mechanism observed in the ground model C2. The failure mechanism was initiated by the collapse of ground beneath the machinery load due to the insufficient of ground bearing capacity, and the surrounding ground was then pushed towards the excavation face. It was considered that the failure mechanism was similar to the bearing capacity failure of foundation. The increase in the maximum excavation depth with the side clearance of the ground model C2 can be observed in the Figure 8.

It should be noted that at the side clearance of 1.75b, the maximum excavation depth is only about 50% of that observed in case of no machinery load (maximum excavation depth of 220 mm). This indicates that the influcenece of the side clearance on the maximum excavation depth is more significant in the ground model C2 than the ground model A and B.

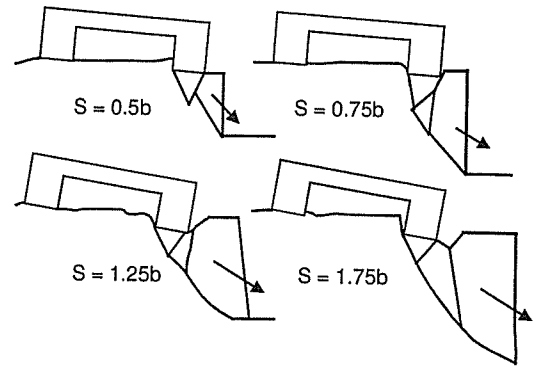

Figure 9. The failure mechanism of the ground model C2

4. CONCLUSIONS

The size and magnitude of the construction machinery load were modelled according to the investigation of drag shovel specifications. The failure mechanisms of trench excavation under the construction machinery load are different depending on the magnitude of bearing pressure of the machinery load and the ultimate bearing capacity of ground. When the bearing pressure of the machinery load was smaller than the ultimate bearing capacity of ground, the failure mechanism was mainly due to the instability of slope. On the other hand, when the bearing pressure was approximately equal to the bearing capacity of ground, the failure mechanism was similarly to the bearing capacity failure of foundation and the effect of the side clearance on the maximum excavation depth was highly significant. In addition, because the construction machinery usually operates under the dynamic condition, further research should be conducted to examine the stability of trench excavation under the dynamic load.

References

Horii, N., Itoh, K., Toyosawa, Y. and Tamate, S. (2006) Development of the NIIS Mark-II geotechnical centrifuge, *International Conference on Physical Modelling on Geotechnique, Hong Kong.* (in press)

Kusakabe, O. (1982) Stability of excavations in soft clay, *Ph.D thesis*, Cambridge University.

Taylor, R.N. (1984) Ground movements associated with tunnels and trenches, *Ph.D thesis*, Cambridge University.

Toyosawa, Y., Horii, N., Tamate, S., Hanayasu, S. and Ampadu, S.K. (1994) Deformation and failure characteristics of vertical cuts and excavations in clay, *Proceeding of International Conference on Centrifuge 94, Singapore*: 663-668.

Toyosawa, Y., Horii, N., and Tamate, S. (1998) Deformation and failure behavior of anchored retaining wall induced by excessive excavation in centrifuge model tests. *NIIS Research report*, NIIS-RR-97: 35-46.

Comparison of Failure Mechanism due to Toe Excavation: Field test, Centrifuge test and Numerical Analysis

S B Tamrakar, Japan National Institute of Occupational Safety and Health, Tokyo, Japan
Y Toyosawa, Japan National Institute of Occupational Safety and Health, Tokyo, Japan
K Itoh, Japan National Institute of Occupational Safety and Health, Tokyo, Japan
T Mitachi, Graduate school of Engineering, Hokkaido University, Hokkaido, Japan

Abstract

To understand the failure mechanism and vertical deformation behavior during the failure of slopes due to excavation, two embankment slopes were prepared in the field from Narita sand (NS) by compaction with bull dozer. Degree of compaction was varied; loose compaction (NSL) and high compaction (NSH). Toe excavation for these embankments were continued until failure occurred by back hoe. Measurement of deformation of the slope top was carried out using invar extensometer and laser beam-optical sensor. These field embankments were modeled in the centrifuge, and in-flight excavator was used to cut the toe of the slopes until failure occurred. Linear vertical differential transducers (LVDTs) were set up on the slope top in the centrifuge model to measure the vertical displacement of slope top. Similarly, numerical analyses were carried out for the field embankments. From numerical analysis, in case of NSL, failure was occurred due to increase in the zone of plastic points from the toe of the slope towards the slope top. Also, zone of plastic points were appeared and increased on the slope top. These zones of plastic points later on combined and final failure occurred. In case of NSH, failure was observed due to increment of plastic zone at the toe and tension cut off zone at the slope top, separately. Accordingly failure pattern in the field for NSL and NSL were different. Finally, vertical displacement was compared. Although some differences in their amount were seen, the displacement pattern after 4^{th} excavation was similar for all the cases.

Keywords: Toe excavation, centrifuge, numerical analysis, PLAXIS, embankment

Introduction

Slope failures are occurred either due to natural phenomenon such as heavy rain or earthquakes or due to human construction works such as slope cutting or excavation or embankment. Failure of slope due to natural phenomenon is unavoidable. But those occurred due to human construction works could be reduced to some extent. Slope failure accidents occurred due to human construction works sometimes takes the lives of the worker and damage the properties around. As shown in Fig. 1,

in Japan accidents (death) due to construction works are reducing every year. In comparison to this, the death accidents those are occurred due to slope failures are not reducing. Every year, about 30 to 40 cases of accidents due to slope failure are recorded. To protect the unstable slope, either retaining wall is constructed or slope is cut to more stable slope angle. But in either case, slope has to be cut. During this cutting or leveling the trench for retaining wall at the toe of the slope, slopes are at the greater risk of failure. In many cases, without any prior signals of failure, sliding occurs instantaneously. Slopes become safe only when the cutting is reached to safer slope or retaining wall construction is completed. More than 50% of slope failure accidents are occurred during cutting or leveling the trench of lower part of the slope.

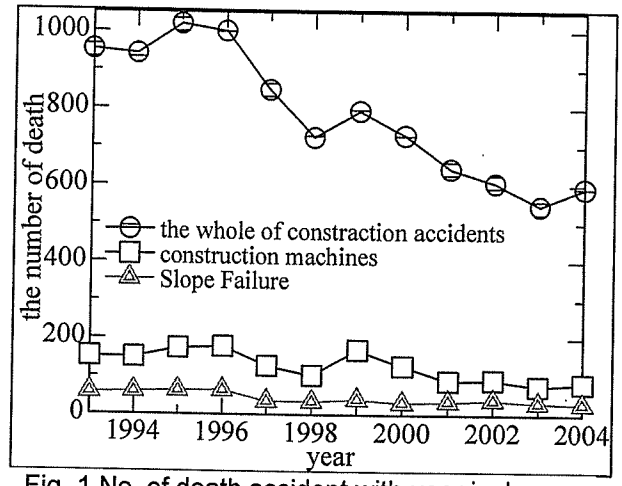

Fig. 1 No. of death accident with year in Japan.

Earlier, Tamrakar et al. (2005 and 2006) had discussed about the failure slope height during the excavation of volcanic sand, Kanto loam and mixture of NSF clay and Toyoura sand slopes. For this, they had performed in-flight excavation in the centrifuge environment and discussed about the difference in the slope failure height while making toe excavation with and without trench excavation at the beginning. Saito et al. (2002), Tamrakar et al (2006), Tamate et al. (2006) and Itoh et al. (2006) had discussed about the methods and instrument of measuring the movement of failure trend just before the failure during excavation in the field. Here, to understand the failure mechanism during field excavation, slope excavation was made at the field and toe excavation was carried out until failure. Then centrifuge in-flight excavation and numerical analyses were carried out for the field embankments so that the failure mechanism and deformation of slope top during the excavation could be made.

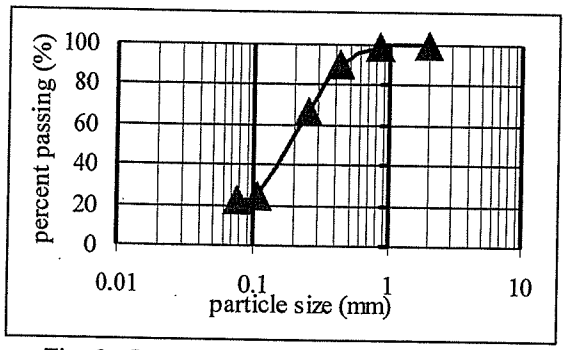

Fig. 2. Grain size distribution curve.

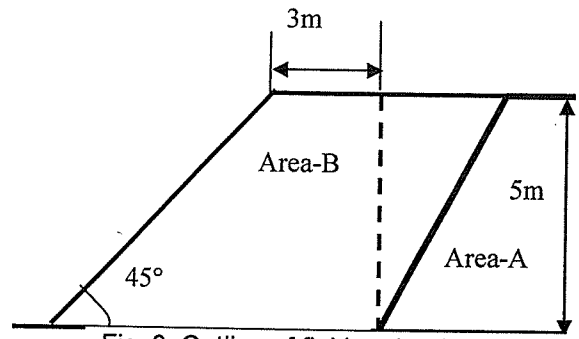

Fig. 3. Outline of field embankment.

1. Field embankments

In the field, four embankments were prepared at Toke (Housing construction site) of Chiba prefecture, Japan (Horii et al. 2006). Here, the two embankments made with Narita sand (NS) are only explained. Narita sand was obtained from the same construction site. Grain size distribution curve is shown in Fig. 2. This soil is classified as SP-G and its soil density (ρ_s) is 2.76 g/cm^3. Embankments were prepared by compacting the soil in layers with the help of a bull dozer (7 tons). Degree of compaction was varied for two types of embankments; lightly compacted one is called NSL and highly compacted one is called NSH. Outline of embankments is shown in Fig. 3. Area A in the figure shows the natural cut while area B shows the embankment constructed. Slope angle is 45° and slope height is 5m with 3.5m width. Photo 1 shows the completed embankments.

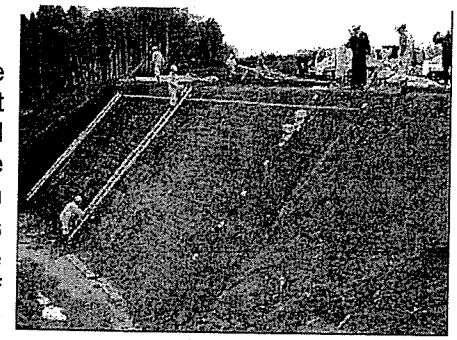
Photo. 1. Field embankment.

For the measurement of the movement of slope top (crest), one invar wire extensometer and a set of laser beam-optical sensor were set up. They were set up at 0.5 m distance from the crest of the embankment. Invar wire extensometer is a commonly used instrument in the field for the

measurement of slope movement which measures the expansion and contraction between two measuring points with the help of stretched invar wire. Laser beam-optical sensor measures the displacements in vertical and horizontal directions with the help of laser beam source and matrix positioned laser receiving optical sensor (refer to Ito et al., 2006). Excavation was started from the toe of the embankment using a back hoe. Excavation was done by inserting the blade on the slope surface vertically downward up to the base and then pulling the blade away from the slope. The width of each cut of excavation was 0.5m and the time interval between two excavation steps was around 5 minutes. Excavation was done until the failure of whole slope took place. For both the embankments, excavation was done up to 6th cut where failure was observed.

2. Centrifuge models

Excavation of field embankments was simulated in the centrifuge. For this, Mark-II centrifuge (Horii et al. 2006) was used. Before preparing the slope models, Narita sand was thoroughly mixed with water content so that water content became almost same as that of filed embankment. Several trial compactions were done to make the wet density of centrifuge model slope equal to those of the field embankments. At the beginning, 5cm thick Kanto loam layer was prepared to represent the natural base as that in field by compacting it under 150 kPa. After this, 20 cm thick model slope ground was prepared in layers. To have uniform density throughout slope, model ground was prepared in 10 layers and 5 minute compaction time was allowed for each layer. In between each layer, NSF clay powder was spread so that inner movement of slope could be observed during excavation and after the failure. Static compaction was done using a bellofragm cylinder. As in the field, here also, two types of centrifuge slope models were prepared. Compaction pressure, wet density and water content for NSL and NSH type centrifuge slope models are shown in Table 1.

Table 1 Centrifuge model test condition.

Embankment type	Compressive stress	wet density	water content
	(kPa)	ρ_t(g/cm^3)	w (%)
NSL	193	1.4	26.1
NSH	265	1.7	25.6

Once the compaction was over, then two sides (wall) of the model box were removed and the model ground was cut to desire slope angle. Dimensions of the model ground are shown in Fig. 4. Here, all the dimensions are scaled to 1/25 to field embankment. Then two sides of the model ground were replaced by glass walls which were provided the marked rubber membranes and thin film of grease which helps to reduce the friction between the glass walls and the model ground. Whole the model box along with model slope was then lowered down on to the centrifuge platform. Linear vertical differential transducers (LVDTs) were set up on the slope top to measure the vertical deformation during the excavation (Photo 2). In case of NSL, they were set up at 1, 4.5, 7.5 and 11cm distances from the slope crest where as for NSH, they were set at 1, 4.5, 7.5 and 10.5cm from the slope crest. LVDTs are generally set up after placing the in-flight excavator above the centrifuge model box.

In-flight excavator (Toyosawa et al., 2000) which can move its blade freely in the vertical (up and down) and horizontal (forward and backward) directions during the running of the centrifuge was used. Since the width of the centrifuge model ground was 20cm, excavating blade of similar size (little less than 20cm) was used. Centrifuge acceleration was then increased in steps from 5, 10, 15, 20, to 25g. Once the deformation became constant at 25g, then excavation was started. Here, to match the field

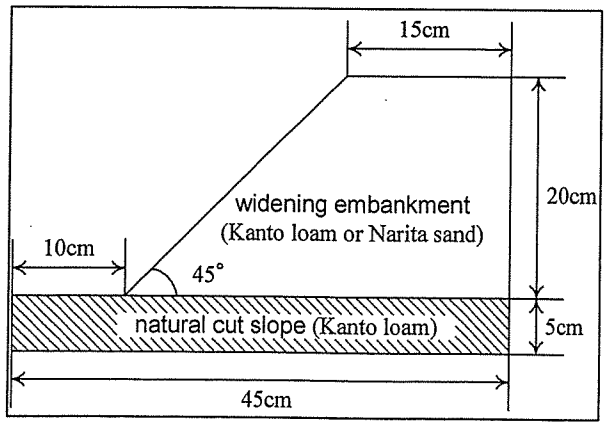

Fig. 4. Dimension of centrifuge model.

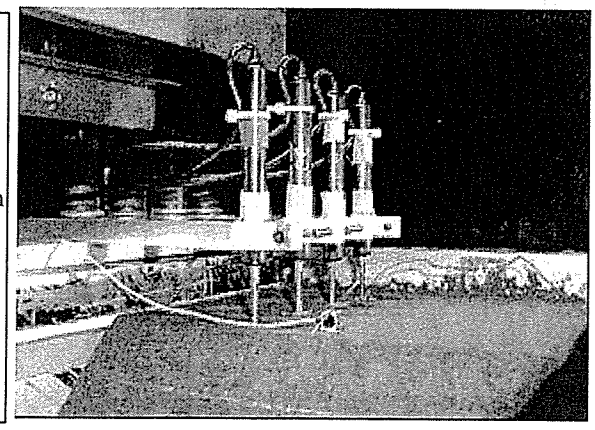

Photo 2. LVDT set up on the top of the model.